ROBUST NQR SIGNAL DETECTION

S. D. Somasundaram, A. Jakobsson† and E. Gudmundson‡*

* King's College London, Division of Engineering, Strand, London, WC2R 2LS, UK
† Karlstad University, Department of Electrical Engineering, SE-651 88 Karlstad, Sweden
‡ Uppsala University, Department of Information Technology, Box 337, SE-751 05 Uppsala, Sweden

ABSTRACT

Nuclear quadrupole resonance (NQR) is a spectroscopic technique that can be used to detect many high explosives and narcotics. Unfortunately, the measured signals are weak, thereby inhibiting the widespread use of the technique. Current state-of-the-art detectors, which exploit realistic NQR data models, assume that the complex amplitudes of the NQR signal components are known, to within a multiplicative constant. However, these amplitudes are typically prone to some level of uncertainty, thus leading to performance loss in these algorithms. Herein, we develop a frequency selective algorithm, robust to uncertainties in the assumed amplitudes, that offers a significant performance gain over current state-of-the art techniques.

Index Terms— Signal detection, robust methods, nuclear quadrupole resonance

1. INTRODUCTION

Nuclear Quadrupole Resonance (NQR) is a radio frequency (RF) spectroscopic technique that can be used to detect the presence of quadrupolar nuclei, such as the ^{14}N nucleus prevalent in many high explosives and narcotics [1–4]. The sample is irradiated with a specially designed sequence of RF pulses and the responses, between pulses, are then measured. The NQR response is highly compound specific, making the technique an important detection tool. Unfortunately, the success of NQR has been hindered by the low signal-to-noise ratio (SNR) signals that are typically observed, especially in the low frequency region, for compounds such as trinitrotoluene (TNT) [5]. Current state-of-the-art detectors, which exploit realistic NQR signal models, assume the complex amplitudes of the NQR signal components are known, to within a multiplicative constant [5–9]. These complex amplitudes are typically obtained from laboratory measurements; however, several factors may cause differences between the assumed complex amplitudes and those observed. For example, in a landmine detection scenario, the field at the sample will vary due to varying distances between the antenna and the mine; consequently, for the same pulse sequence parameters and RF power, the flip-angle(s) of the excited resonant line(s) will also vary, causing variations in the NQR signal amplitudes. Typically, such variations will reduce the performance of these detectors (see also [10]). Therefore, we here proceed to derive a robust algorithm that finds the best complex amplitude vector within a hypersphere of uncertainty around a specified complex amplitude vector. The approach allows for inclusion of prior information, both via the specified complex amplitude vector and via the selection of the size of the uncertainty region. We also propose a method for selecting the size of the uncertainty region, based upon knowledge of the uncertainties of the complex amplitudes. Furthermore, to reduce computational complexity and provide robustness to RF interference, the detector is formed using only those spectral bands where the NQR signal components are expected to lie. Extensive numerical analysis using both simulated and measured data, obtained from a sample of TNT, indicate that the proposed detector offers a significantly increased detection performance as compared to current state-of-the-art detectors.

This work was supported in part by the Defence Science and Technology Laboratory (DSTL) at Fort Halstead, UK, and the Swedish Research Council.

‡ Corresponding author. E-mail: erik.gudmundson@it.uu.se.

2. DATA MODEL

In [5–7], a model for the NQR echo train, as produced by a pulsed spin locking sequence, was presented. The NQR signal is typically embedded in coloured noise, which can be well modelled as an autoregressive (AR) process. Without loss of generality, the prewhitened data model may be written as

$$z^m(t) = \rho \sum_{k=1}^{d} \bar{C}\kappa_k e^{-\eta_k(t+m\mu)} e^{-\beta_k|t-t_{sp}|+i\omega_k(T)t} + e^m(t), \quad (1)$$

where $t = t_0, \ldots, t_{N-1}$ is the echo sampling time. Furthermore, $m = 0, \ldots, M-1$ is the echo number; t_{sp} is the echo peak offset; the echo spacing $\mu = 2t_{sp}$; ρ is the common scaling due to the signal power; κ_k, β_k and η_k denote the normalised (complex) amplitude, the sinusoidal damping constant and echo train damping constant of the kth NQR frequency, respectively. Often, information about each κ_k is available for a given substance and experimental set-up. The sinusoidal and echo damping constants, β_k and η_k, are here modelled as unknown parameters. Furthermore, $\omega_k(T)$ is the frequency shifting function of the kth NQR frequency component which, in general, depends on the *unknown* temperature, T, of the examined sample. An important point to note is that the number of sinusoidal components, d, as well as the frequency shifting function for each spectral line, $\omega_k(T)$, may be assumed to be *known*. For many substances, such as TNT, the frequency shifting function(s), over the temperatures of interest, can be well modelled as linear functions, i.e., [4]

$$\omega_k(T) = a_k - b_k T, \quad (2)$$

where a_k and b_k, for $k = 1, \ldots, d$, are given constants. The complex scaling, due to the prewhitening operation, may be written as $\bar{C} = C(\lambda_k)$ for $\lfloor t - t_{sp} \rfloor < 0$, otherwise $\bar{C} = C(\tilde{\lambda}_k)$, where $\lfloor x \rfloor$ denotes the integer part of x, $\lambda_k = e^{i\omega_k(T)+\beta_k-\eta_k}$ and $\tilde{\lambda}_k = e^{i\omega_k(T)-\beta_k-\eta_k}$. Furthermore, $C(\lambda)$ denotes the AR prewhitening filter (see [8] for further details). Finally, $e^m(t)$ is an additive *white* noise.

3. THE FRETAML DETECTOR

Using (1), the mth prewhitened echo may be written as

$$\mathbf{z}_N^m \triangleq \left[\begin{array}{ccc} z^m(t_0) & \dots & z^m(t_{N-1}) \end{array}\right]^T = \rho \mathbf{A}_{\bar{\boldsymbol{\theta}}}\mathbf{B}_m\boldsymbol{\kappa} + \mathbf{e}_N^m, \quad (3)$$

where $\mathbf{e}_N^m$ is defined similar to $\mathbf{z}_N^m$, and

$$\begin{aligned}
\mathbf{A}_{\bar{\boldsymbol{\theta}}} &= \begin{bmatrix} C(\lambda_1)S_{1,t_0} & \cdots & C(\lambda_d)S_{d,t_0} \\ \vdots & \ddots & \vdots \\ C(\lambda_1)S_{1,\tilde{t}_{sp}} & \cdots & C(\lambda_d)S_{d,\tilde{t}_{sp}} \\ C(\tilde{\lambda}_1)S_{1,\tilde{t}_{sp}+1} & \cdots & C(\tilde{\lambda}_d)S_{d,\tilde{t}_{sp}+1} \\ \vdots & \ddots & \vdots \\ C(\tilde{\lambda}_1)S_{1,t_{N-1}} & \cdots & C(\tilde{\lambda}_d)S_{d,t_{N-1}} \end{bmatrix} \\
\mathbf{B}_m &= \text{diag}\{e^{-\eta_1 m}, \dots, e^{-\eta_d m}\} \\
\boldsymbol{\kappa} &= [\kappa_1 \cdots \kappa_d]^T,
\end{aligned}$$

where $\tilde{t}_{sp}$ is the closest data point such that $\tilde{t}_{sp} \leq t_{sp}$. Furthermore, $S_{k,t} = e^{[i\omega_k(T)-\eta_k]t}e^{-\beta_k|t-t_{sp}|}$, the upper block of $\mathbf{A}_{\bar{\boldsymbol{\theta}}}$ is $(\lfloor t_{sp} - t_0 \rfloor) \times d$ and the lower block is $(N - \lfloor t_{sp} - t_0 \rfloor) \times d$, and $\bar{\boldsymbol{\theta}} = [T\ \boldsymbol{\beta}^T\ \boldsymbol{\eta}^T]^T$, where $\boldsymbol{\beta}$ and $\boldsymbol{\eta}$ denote the vectors of unknown sinusoidal and echo dampings, respectively. As the temperature of the sample can be assumed to lie in a known temperature range, we may, using (2), determine the range of frequencies each sinusoidal component may be present in. Hence, a frequency selective detector that only considers these narrow frequency bands can be derived. Consider selecting the frequency regions formed by

$$\left\{\frac{2\pi k_1}{N}, \frac{2\pi k_2}{N}, \dots, \frac{2\pi k_L}{N}\right\}, \quad (4)$$

with $k_1, \dots, k_L$ being L given, not necessarily consecutive, integers selected such that (4) only consists of the possible frequency grid points for each of the d signal components. For the mth echo, the Fourier transformed (prewhitened) data vector, consisting only of the frequency regions in (4), can be expressed as

$$\mathbf{Z}_L^m \triangleq \left[Z_{k_1}^m \cdots Z_{k_L}^m\right]^T = \rho \mathbf{V}_L^* \mathbf{A}_{\bar{\boldsymbol{\theta}}}\mathbf{B}_m\boldsymbol{\kappa} + \mathbf{E}_L^m, \quad (5)$$

where

$$\mathbf{V}_L = [\mathbf{v}_{k_1} \cdots \mathbf{v}_{k_L}]\ ;\ \mathbf{v}_{k_j} = \left[1\ \ e^{i2\pi\frac{k_j}{N}}\ \cdots\ e^{i2\pi\frac{k_j(N-1)}{N}}\right]^T. \quad (6)$$

Finally, $\mathbf{E}_L^m$, defined similarly to $\mathbf{Z}_L^m$, is the transformed noise sequence associated with the mth echo. Using (5), the (frequency selected) transformed data model for the whole echo train can be expressed as

$$\mathbf{Z}_{LM} \triangleq \left[(\mathbf{Z}_L^0)^T \cdots (\mathbf{Z}_L^{M-1})^T\right]^T = \rho\, \tilde{\mathbf{H}}_{\bar{\boldsymbol{\theta}}}\boldsymbol{\kappa} + \mathbf{E}_{LM}, \quad (7)$$

where $\mathbf{E}_{LM}$ is defined similar to $\mathbf{Z}_{LM}$, and

$$\tilde{\mathbf{H}}_{\bar{\boldsymbol{\theta}}} = \begin{bmatrix} \mathbf{V}_L^*\mathbf{A}_{\bar{\boldsymbol{\theta}}}\mathbf{B}_0 \\ \vdots \\ \mathbf{V}_L^*\mathbf{A}_{\bar{\boldsymbol{\theta}}}\mathbf{B}_{M-1} \end{bmatrix}. \quad (8)$$

The (approximate) maximum likelihood estimate of $\boldsymbol{\theta} = [\rho, \boldsymbol{\kappa}, \bar{\boldsymbol{\theta}}]$ can be found as

$$\hat{\boldsymbol{\theta}} = \arg\min_{\boldsymbol{\theta}} \left\| \ \mathbf{Z}_{LM} - \rho\tilde{\mathbf{H}}_{\bar{\boldsymbol{\theta}}}\boldsymbol{\kappa}\ \right\|_2^2, \quad (9)$$

where $\|\cdot\|_2$ denotes the two-norm. We note that from a computational point of view, it is possible to exploit the fact that the indices of $\mathbf{V}_L^*\mathbf{A}_{\bar{\boldsymbol{\theta}}}\mathbf{B}_m$ form geometric series (see [10] for more details). Assuming known $\bar{\boldsymbol{\theta}}$, an initial estimate of ρ can be obtained as $\hat{\rho} = \max_k\{|(\tilde{\mathbf{H}}_{\bar{\boldsymbol{\theta}}})^\dagger \mathbf{Z}_{LM}|\}$, where $\mathbf{X}^\dagger \triangleq (\mathbf{X}^*\mathbf{X})^{-1}\mathbf{X}^*$ is the Moore-Penrose pseudoinverse. To allow for uncertainties in the assumed amplitude vector $\bar{\boldsymbol{\kappa}}$, we assume that both $\bar{\boldsymbol{\kappa}}$ and the true amplitude vector, $\boldsymbol{\kappa}$, will belong to an uncertainty hypersphere with radius $\sqrt{\epsilon}$ (compare with [11]). An estimate of $\boldsymbol{\kappa}$ can then be found by solving the following constrained minimisation

$$\min_{\boldsymbol{\kappa}} \left\|\hat{\rho}\tilde{\mathbf{H}}_{\bar{\boldsymbol{\theta}}}\boldsymbol{\kappa} - \mathbf{Z}_{LM}\right\|_2^2 \text{ subject to } \left\|\boldsymbol{\kappa} - \bar{\boldsymbol{\kappa}}\right\|_2^2 \leq \epsilon. \quad (10)$$

This optimisation can be solved via the singular value decomposition (SVD). Firstly, the SVD of $\tilde{\mathbf{H}}_{\bar{\boldsymbol{\theta}}}$ is computed as

$$\tilde{\mathbf{H}}_{\bar{\boldsymbol{\theta}}} = \mathbf{U}\boldsymbol{\Sigma}\mathbf{V}^*, \quad (11)$$

where $\mathbf{U} \in C^{LM\times r}$, $\boldsymbol{\Sigma} \in R^{r\times r}$ and $\mathbf{V} \in C^{d\times r}$, with $r = \text{rank}(\tilde{\mathbf{H}}_{\bar{\boldsymbol{\theta}}})$. We note that $\tilde{\mathbf{H}}_{\bar{\boldsymbol{\theta}}}$ has full column rank, therefore $r = d$. Furthermore, $\boldsymbol{\Sigma} = \text{diag}\{\sigma_1, \dots, \sigma_d\}$, where σ_j denotes the jth singular value, and $\mathbf{U}$ and $\mathbf{V}$ are unitary matrices. Using the SVD of $\tilde{\mathbf{H}}_{\bar{\boldsymbol{\theta}}}$, (10) can be written as

$$\begin{gathered}
\min_{\tilde{\boldsymbol{\kappa}}} \left\|\hat{\rho}\boldsymbol{\Sigma}\tilde{\boldsymbol{\kappa}} - \tilde{\mathbf{Z}}\right\|_2^2 \text{ subject to } \left\|\mathbf{V}[\tilde{\boldsymbol{\kappa}} - \tilde{\bar{\boldsymbol{\kappa}}}]\right\|_2^2 \leq \epsilon \\
\Leftrightarrow \\
\min_{\tilde{\boldsymbol{\kappa}}} \sum_{j=1}^d \left|\hat{\rho}\sigma_j\tilde{\kappa}_j - \tilde{Z}_j\right|^2 \text{ subject to } \sum_{j=1}^d \left|\tilde{\kappa}_j - \tilde{\bar{\kappa}}_j\right|^2 \leq \epsilon,
\end{gathered} \quad (12)$$

where $\tilde{\mathbf{Z}} = \mathbf{U}^*\mathbf{Z}_{LM}$, $\tilde{\boldsymbol{\kappa}} = \mathbf{V}^*\boldsymbol{\kappa}$ and $\tilde{\bar{\boldsymbol{\kappa}}} = \mathbf{V}^*\bar{\boldsymbol{\kappa}}$. Furthermore, $\tilde{\kappa}_j$, $\tilde{Z}_j$ and $\tilde{\bar{\kappa}}_j$ denote the jth components of $\tilde{\boldsymbol{\kappa}}$, $\tilde{\mathbf{Z}}$ and $\tilde{\bar{\boldsymbol{\kappa}}}$, respectively. It is clear that

$$\tilde{\kappa}_j \triangleq \tilde{Z}_j/(\hat{\rho}\sigma_j) \quad (13)$$

is a minimiser of the objective function. If it also satisfies the constraint equation (i.e., if the vector is feasible), then we have a solution to (12). However, if the vector does not satisfy the constraint, the solution will lay on the boundary of the feasible set [12]. For this case, (12) can be solved using the method of Lagrange multipliers. Defining

$$L(\lambda, \tilde{\boldsymbol{\kappa}}) = \left\|\hat{\rho}\boldsymbol{\Sigma}\tilde{\boldsymbol{\kappa}} - \tilde{\mathbf{Z}}\right\|_2^2 + \lambda\left(\left\|\mathbf{V}[\tilde{\boldsymbol{\kappa}} - \tilde{\bar{\boldsymbol{\kappa}}}]\right\|_2^2 - \epsilon\right), \quad (14)$$

where λ is the Lagrange multiplier, the equations $\partial L(\lambda, \tilde{\boldsymbol{\kappa}})/\partial\tilde{\kappa}_j^* = 0$, $j = 1, \dots, d$, lead to the linear system

$$\left(|\hat{\rho}|^2\boldsymbol{\Sigma}^*\boldsymbol{\Sigma} + \lambda\mathbf{I}\right)\tilde{\boldsymbol{\kappa}} = \hat{\rho}^*\boldsymbol{\Sigma}^*\tilde{\mathbf{Z}} + \lambda\tilde{\bar{\boldsymbol{\kappa}}}. \quad (15)$$

As $(|\hat{\rho}|^2\boldsymbol{\Sigma}^*\boldsymbol{\Sigma} + \lambda\mathbf{I})$ is guaranteed to be nonsingular, the solution is given by

$$\tilde{\kappa}_j(\lambda) = \frac{\hat{\rho}^*\sigma_j^*\tilde{Z}_j + \lambda\tilde{\bar{\kappa}}_j}{|\hat{\rho}\sigma_j|^2 + \lambda}. \quad (16)$$

To find the value of the Lagrange multiplier, we define

$$\phi(\lambda) = \left\|\mathbf{V}[\tilde{\boldsymbol{\kappa}} - \tilde{\bar{\boldsymbol{\kappa}}}]\right\|_2^2 = \sum_{j=1}^d \left|\frac{\hat{\rho}^*\sigma_j^*\tilde{Z}_j - |\hat{\rho}\sigma_j|^2\tilde{\bar{\kappa}}_j}{|\hat{\rho}\sigma_j|^2 + \lambda}\right|^2, \quad (17)$$

noting that it is a monotonically decreasing function of λ, and that $\phi(0) > \epsilon$. These observations imply that there is a unique $\hat{\lambda}$ such that $\phi(\hat{\lambda}) = \epsilon$. The root can easily be found using any standard root-finding technique, e.g., Newton's method. The required solution to

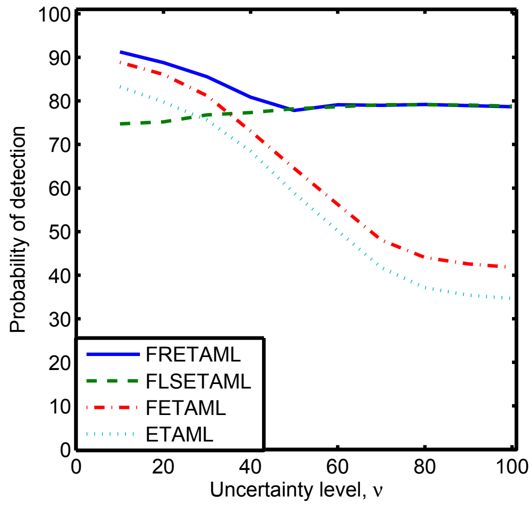

Fig. 1. Plots illustrating the probability of detection, p_d, as a function of uncertainty, ν, using simulated data.

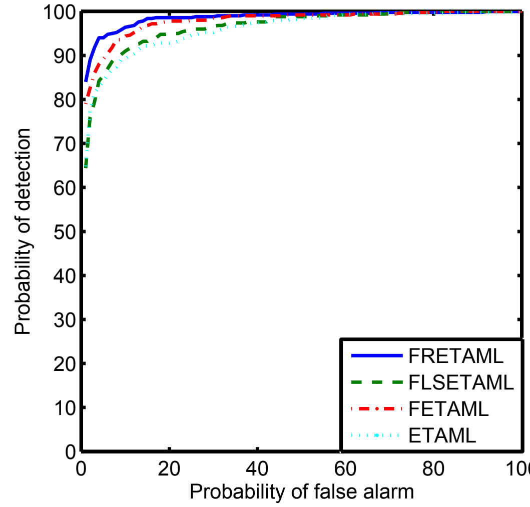

Fig. 2. The ROC curves comparing detectors using measured data.

the original constrained minimisation (10) is then given as

$$\hat{\boldsymbol{\kappa}} = \mathbf{V}\tilde{\boldsymbol{\kappa}}, \tag{18}$$

where $\hat{\boldsymbol{\kappa}}$ is the robust estimate of $\boldsymbol{\kappa}$. Given $\hat{\boldsymbol{\kappa}}$, we may re-estimate ρ as $\hat{\hat{\rho}} = (\tilde{\mathbf{H}}_{\bar{\boldsymbol{\theta}}}\hat{\boldsymbol{\kappa}})^{\dagger}\mathbf{Z}_{LM}$. Substituting these estimates into the norm in (9) yields the residual least squares error

$$\left\| \ \mathbf{Z}_{LM} - \hat{\hat{\rho}}\tilde{\mathbf{H}}_{\bar{\boldsymbol{\theta}}}\hat{\boldsymbol{\kappa}} \ \right\|_2^2 = \mathbf{Z}_{LM}^*\mathbf{Z}_{LM} - \mathbf{Z}_{LM}^*\mathbf{\Pi}_{\tilde{\mathbf{H}}_{\bar{\boldsymbol{\theta}}}\hat{\boldsymbol{\kappa}}}\mathbf{Z}_{LM}, \tag{19}$$

where $\mathbf{\Pi}_{\tilde{\mathbf{H}}_{\bar{\boldsymbol{\theta}}}\hat{\boldsymbol{\kappa}}} = (\tilde{\mathbf{H}}_{\bar{\boldsymbol{\theta}}}\hat{\boldsymbol{\kappa}})(\tilde{\mathbf{H}}_{\bar{\boldsymbol{\theta}}}\hat{\boldsymbol{\kappa}})^{\dagger}$. Thus, for each $\bar{\boldsymbol{\theta}}$, a new estimate of $\boldsymbol{\kappa}$ is obtained, and as a result, a new value of $\mathbf{Z}_{LM}^*\mathbf{\Pi}_{\tilde{\mathbf{H}}_{\bar{\boldsymbol{\theta}}}\hat{\boldsymbol{\kappa}}}\mathbf{Z}_{LM}$. The $\bar{\boldsymbol{\theta}}$ associated with the maximum value of $\mathbf{Z}_{LM}^*\mathbf{\Pi}_{\tilde{\mathbf{H}}_{\bar{\boldsymbol{\theta}}}\hat{\boldsymbol{\kappa}}}\mathbf{Z}_{LM}$ yields the estimate of $\bar{\boldsymbol{\theta}}$. Given the estimate of $\bar{\boldsymbol{\theta}}$, we proceed to form the test statistic, $T(\mathbf{Z}_{LM})$, as the (approximative) generalized likelihood ratio test for a signal with unknown noise variance, i.e.,

$$T(\mathbf{Z}_{LM}) = (2LM-1)\frac{\mathbf{Z}_{LM}^*\mathbf{\Pi}_{\tilde{\mathbf{H}}_{\bar{\boldsymbol{\theta}}}\hat{\boldsymbol{\kappa}}}\mathbf{Z}_{LM}}{\mathbf{Z}_{LM}^*(\mathbf{I}-\mathbf{\Pi}_{\tilde{\mathbf{H}}_{\bar{\boldsymbol{\theta}}}\hat{\boldsymbol{\kappa}}})\mathbf{Z}_{LM}}. \tag{20}$$

Using (20), the signal component is deemed present if and only if $T(\mathbf{Z}_{LM}) > \gamma$, and otherwise not, where γ, computed from the noise-only data, is a predetermined threshold value reflecting the acceptable probability of false alarm (p_f). As noted in [6], several simplifications can be made to this detector by using different strategies to evaluate the $(2d+1)$–dimensional search. It was noted in [8], that approximating the sinusoidal damping parameters to be the same does not alter detector performance significantly. Therefore, letting $\beta_k \approx \beta_0$ reduces the search dimension to $(d+2)$ over the unknown echo damping parameters, temperature and the common sinusoidal damping parameter. Furthermore, as noted in [6, 8, 9], this full $(d+2)$–dimensional search may be well approximated using $(d+2)$ 1–dimensional searches, which may be iterated to further improve the fitting. We denote the resulting detector the frequency selective robust echo train approximative maximum likelihood (FRETAML) detector.

4. THE SIZE OF THE UNCERTAINTY REGION

From the above discussion, it is clear that the choice of the radius of the uncertainty hypersphere, $\sqrt{\epsilon}$, will significantly affect the estimate of $\boldsymbol{\kappa}$. We will now consider this issue in further detail. One approach is to use laboratory measurements to examine various performance measures, e.g., the receiver operator characteristic (ROC), for different values of ϵ, using these measures to determine a suitable value for ϵ. However, we can also get an idea of the value of ϵ from the constraint equation in (10) and by making assumptions about the uncertainties in the complex amplitudes. Firstly, we rewrite κ_k as

$$\kappa_k = (|\bar{\kappa}_k| + \Delta_k^m)e^{i(\angle\bar{\kappa}_k + \Delta_k^p)}, \tag{21}$$

where $|\bar{\kappa}_k|$ and $\angle\bar{\kappa}_k$ denote the *assumed* magnitude and phase components of the kth complex amplitude, respectively; Δ_k^m and Δ_k^p denote the errors in the kth magnitude and phase components, respectively. The magnitude errors, Δ_k^m, are here assumed to be independent truncated Gaussian random variables whose distributions are each given by the conditional probability density function (PDF),

$$f\left(\Delta_k^m \,\middle|\, \Delta_k^m > -|\bar{\kappa}_k|\right) = \frac{f(\Delta_k^m)}{1-F(-|\bar{\kappa}_k|)}, \tag{22}$$

where the PDF, $f(x)$, is a zero mean Gaussian density, with variance σ_m^2, and $F(x)$ is its corresponding distribution function. The phase errors, Δ_k^p, are here assumed to be independent identically distributed random variables, uniformly distributed over the interval $[-P, P]$, where $0 \le P \le \pi$ is selected according to the uncertainty in the phases. The PDF of Δ_k^p is thus given as

$$f(\Delta_k^p) = \begin{cases} \frac{1}{2P} & -P < \Delta_k^p \le P \\ 0 & \text{Otherwise.} \end{cases} \tag{23}$$

A reasonable way to form ϵ can then be

$$\epsilon = \left\|\boldsymbol{\kappa} - \bar{\boldsymbol{\kappa}}\right\|_2^2 = \sum_{k=1}^{d}\left|\kappa_k - \bar{\kappa}_k\right|^2, \tag{24}$$

with $\boldsymbol{\kappa}$ defined as in (21). As noted in [10], a good choice of ϵ is the mean of (24), which can be evaluated via Monte-Carlo simulations. For simplicity, we define the uncertainty parameter, ν, which couples both the uncertainties in the phases and the magnitudes. For a given value of ν, we set $P = \pi \frac{\nu}{100}$ and $\sigma_m^2 = 0.0001\nu$.

5. NUMERICAL EXAMPLES

In this section, we examine the performance of the proposed detector using both simulated and measured NQR data. The real data consisted of 1000 data files, 500 with TNT present and 500 without, each file taking around one minute to acquire. Each file consisted of four echo trains summed up and phase cycled, to reduce baseline offset. The echo trains were made up of $M = 26$ echoes, each consisting of $N = 256$ samples. The sample, which consisted of 180g creamed monoclinic TNT, was placed inside a shielded solenoidal coil. The temperature of the sample was not artificially controlled, but can be assumed to be around 297 K (see [10] for further experimental details). Table 1 summarises the NQR signal parameters, estimated from the signal as obtained by summing all the 2000 TNT echo trains. Furthermore, the experimental settings were such that the noise could be assumed white. The temperature shifting functions for the $d = 4$ lines of monoclinic TNT are $a_1 = 893.502$, $a_2 = 875.734$, $a_3 = 892.503$, $a_4 = 870.293$ (all a_k in kHz), $b_1 = 0.1529$, $b_2 = 0.1070$, $b_3 = 0.1685$ and $b_4 = 0.1125$ (all b_k in kHzK^{-1}) [8]. The detectors were also compared using simulated data, which was generated using (1), (2) together with the temperature shifting functions, and the values in Table 1. For the simulated data, the number of Monte-Carlo simulations was 1500 and the SNR was -28 dB, where SNR is defined as SNR $= \sigma_e^{-2}\sigma_s^2$, with σ_e^2 and σ_s^2 denoting the power of the noise and the noise-free signal, respectively. In the following analysis, we compare the proposed FRETAML algorithm to the ETAML and FETAML algorithms, presented in [6], together with the FLSETAML detector which estimates $\boldsymbol{\kappa}$ using (13) and (18). The detectors used the following search regions (see, e.g., [6] for further explanations on how to choose the search regions); the search region over temperature was selected as $T = [292, 302]$ K (in 100 steps), the common sinusoidal damping parameter and the echo train damping parameters used $\beta_0 = [0.001, 0.1]$ and $\eta_k = [0.0002, 0.0004]$ (both in 100 steps), respectively. Figure 1 illustrates the probability of detection (p_d) as a function of the uncertainty level, ν, using simulated data, for probability of false alarm (p_f) of 1%. For each uncertainty level, ϵ was chosen as the mean of (24), calculated using 10^7 Monte-Carlo simulations. The estimated mean values for $\nu = 10, 20, 30, 40, 50, 60, 70, 80, 90$ and 100% are 0.0826, 0.3180, 0.6925, 1.1846, 1.7661, 2.4046, 3.0653, 3.7124, 4.3162, and 4.8452, respectively. The figure shows that the proposed robust detector outperforms the other detectors for all uncertainty levels; this as the robust detector is able to incorporate prior knowledge, whilst also allowing for uncertainties in it. We proceed to examine the ROC curves for the different detectors, using the real data. We note that the data was measured under laboratory conditions where only the temperature was allowed to vary. Therefore, the error between $\bar{\boldsymbol{\kappa}}$ and $\boldsymbol{\kappa}$ can be expected to be low. Figure 2 illustrates the ROC curves, where $\bar{\boldsymbol{\kappa}}$ is constructed from estimates of the complex amplitudes, summarised in Table 1, with $\epsilon = 0.5$. The figure illustrates that there is a gain for the proposed robust detector, even for the case when the uncertainty in $\bar{\boldsymbol{\kappa}}$ is very low.[1]

[1]The authors are grateful to Professor John A. S. Smith and Mr. Richard Silversides, from King's College, London, for useful suggestions.

Table 1. Estimates of NQR signal parameters for the $d = 4$ NQR components of monoclinic TNT, for an excitation frequency of 841.5 kHz, in the region of 830-860 kHz

k	1	2	3	4
β_k	0.0048	0.0049	0.0046	0.0038
$\eta_k \times 10^{-3}$	0.2126	0.2096	0.2237	0.2576
$\lvert\kappa_k\rvert$	0.39	0.88	1	0.69
$\angle\kappa_k$ (rads)	-0.7546	-2.9428	-0.7541	-1.0870

6. REFERENCES

[1] J. A. S. Smith, "Nitrogen-14 Quadrupole Resonance Detection of RDX and HMX Based Explosives," *European Convention on Security and Detection*, vol. 408, pp. 288–292, 1995.

[2] M. D. Rowe and J. A. S. Smith, "Mine Detection by Nuclear Quadrupole Resonance," *The Detection of Abandoned Landmines (IEE) Eurel*, vol. 43, pp. 62–66, 1996.

[3] A. N. Garroway, M. L. Buess, J. B. Miller, B. H. Suits, A. D. Hibbs, A. G. Barrall, R. Matthews, and L. J. Burnett, "Remote Sensing by Nuclear Quadrupole Resonance," *IEEE Trans. Geoscience and Remote Sensing*, vol. 39, no. 6, pp. 1108–1118, June 2001.

[4] R. M. Deas, I. A. Burch, and D. M. Port, "The Detection of RDX and TNT Mine like Targets by Nuclear Quadruple Resonance," in *Detection and Remediation Technologies for Mines and Minelike Targets, Proc. of SPIE*, 2002, vol. 4742, pp. 482–489.

[5] S. D. Somasundaram, A. Jakobsson, J. A. S. Smith, and K. A. Althoefer, "Frequency Selective Detection of Nuclear Quadrupole Resonance (NQR) Spin Echoes," in *Detection and Remediation Technologies for Mines and Minelike Targets XI, Proc. of SPIE*, 2006, vol. 6217.

[6] S. D. Somasundaram, A. Jakobsson, J. A. S. Smith, and K. Althoefer, "Exploiting Spin Echo Decay in the Detection of Nuclear Quadrupole Resonance Signals," To appear in *IEEE Trans. Geoscience and Remote Sensing.*

[7] J. A. S. Smith, S. D. Somasundaram, A. Jakobsson, M. Mossberg, and M. D. Rowe, "Method of Apparatus for NQR testing," *WO2006064264.*

[8] A. Jakobsson, M. Mossberg, M. Rowe, and J. Smith, "Exploiting Temperature Dependency in the Detection of NQR Signals," *IEEE Trans. Signal Processing*, vol. 54, no. 5, pp. 1610–1616, May 2006.

[9] A. Jakobsson, M. Mossberg, M. Rowe, and J. A. S. Smith, "Frequency Selective Detection of Nuclear Quadrupole Resonance Signals," *IEEE Trans. Geoscience and Remote Sensing*, vol. 43, no. 11, pp. 2659–2665, November 2005.

[10] S. D. Somasundaram, A. Jakobsson, and E. Gudmundson, "Robust NQR Signal Detection Allowing for Amplitude Uncertainties," Submitted to *IEEE Trans. Signal Processing*.

[11] J. Li, P. Stoica, and Z. Wang, "On Robust Capon Beamforming and Diagonal Loading," *IEEE Trans. on Signal Processing*, vol. 51, no. 7, pp. 1702–1715, July 2003.

[12] G. H. Golub and C. F. Van Loan, *Matrix Computations*, The John Hopkins University Press, 3^{rd} edition, 1996.